mathematics

MDPI

Article

Utilization of a Genetic Algorithm to Identify Optimal Geometric Shapes for a Seismic Protective Barrier

Vladimir Bratov [1,*], Andrey Murachev [2] and Sergey V. Kuznetsov [3]

[1] School of Computing, Engineering & The Built Environment, Edinburgh Napier University, Edinburgh EH10 5DT, UK
[2] Department of Theoretical Mechanics, Peter the Great St. Petersburg Polytechnic University, St. Petersburg 195251, Russia; andrey.murachev@spbstu.ru
[3] Ishlinsky Institute for Problems in Mechanics, Moscow 119526, Russia; kuzn-sergey@yandex.ru
* Correspondence: v.bratov@napier.ac.uk

Abstract: The utilization of seismic barriers for protection against the hazardous impact of natural or technogenic waves is an extremely promising emerging technology to secure buildings, structures and entire areas against earthquake-generated seismic waves, high-speed-transport-induced vibrations, etc. The current research is targeted at studying the effect of seismic-barrier shape on the reduction of seismic-wave magnitudes within the protected region. The analytical solution of Lamb's problem was used to verify the adopted numerical approach. It was demonstrated that the addition of complementary geometric features to a simple barrier shape provides the possibility of significantly increasing the resulting seismic protection. A simple genetic algorithm was employed to evaluate the nontrivial but extremely effective geometry of the seismic barrier. The developed approach can be used in various problems requiring optimization of non-parameterizable geometric shapes. The applicability of genetic algorithms and other generative algorithms to discover optimal (or close to optimal) geometric configurations for the essentially multiscale problems of the interaction of mechanical waves with inclusions is discussed.

Keywords: seismic barrier; earthquake; vibration; complex geometry; genetic algorithm; optimization; multiscale modeling; heterogeneous media and structures

MSC: 74P10; 74J25; 74H15

Citation: Bratov, V.; Murachev, A.; Kuznetsov, S.V. Utilization of a Genetic Algorithm to Identify Optimal Geometric Shapes for a Seismic Protective Barrier. *Mathematics* **2024**, *12*, 492. https://doi.org/10.3390/math12030492

Academic Editor: Ioannis G. Tsoulos

Received: 7 December 2023
Revised: 26 January 2024
Accepted: 29 January 2024
Published: 4 February 2024

1. Introduction

The use of seismic barriers to protect buildings and structures from the potentially harmful energy of surface waves of natural or technogenic origin is a relatively new emerging approach in modern seismic protection developments. In contrast to the traditional approaches, which, in most cases, rely on the installation of damping between the structure basement and the structure itself, the considered seismic barriers provide the possibility of ensuring territorial protection, significantly reducing the amplitude of displacements and accelerations in the area encircled by the barrier and embracing protected buildings and structures. Installation of a seismic barrier makes it possible to ensure the required levels of protection for buildings and structures inside the protected area, and it possesses a number of significant advantages over more traditional seismic protection methods. The major advantages of the considered territorial seismic protection include the following:

- Barriers protect the area on which the structure is placed, along with the structure itself;
- Seismic barriers are not a part of the protected structure; thus, degradation and fracture of barriers do not directly affect the strength and stability of the structure;
- The functionality of the barrier is not significantly affected by the frequency spectrum of oncoming seismic waves (unlike more traditional seismic protection systems that are designed to operate in a certain frequency range);

- Basement slabs are also protected;
- Barriers can be used to protect structures placed on weak soils that potentially can be exposed to the earthquake-induced liquefaction (as seismic barriers prevent the propagation of seismic waves into the protected area);
- Barriers can be retrofitted to protect the existing structures;
- In many cases, the creation of seismic barriers is economically much more efficient compared with the more traditional seismic protection systems.

The potential of various seismic protective structures based on specially designed metamaterials [1–7], seismic barriers [1,7–16], or even seismic barriers filled with metamaterials [2,4,5,8] was explicitly revealed in a large number of previous works. Earlier research clearly demonstrates the possibility of using seismic barriers for effective protection against seismic waves of different origins. A seismic barrier represents a vertical inclusion made from a material having physical properties different from the ambient medium. The interaction of the incident wave with this inclusion (seismic barrier) can result in the diffraction, reflection, refraction and scattering of waves. In addition to this, part of the wave energy can be captured inside the barrier. These effects can result in a decrease in wave amplitude behind the barrier. A schematic representation of the vertical barrier is given in Figure 1: A time-dependent load $P(t)$ is initiating a wave travelling along the surface of a half-plane simulating the effect of an earthquake at areas not directly adjacent to the earthquake epicentre; the seismic barrier (black rectangular area in Figure 1) interacts with a seismic wave caused by the applied dynamic surface load, which generates surface Rayleigh waves along with bulk waves emanating from the point force load; the wave amplitudes are measured by a sensor located on the free surface behind the barrier.

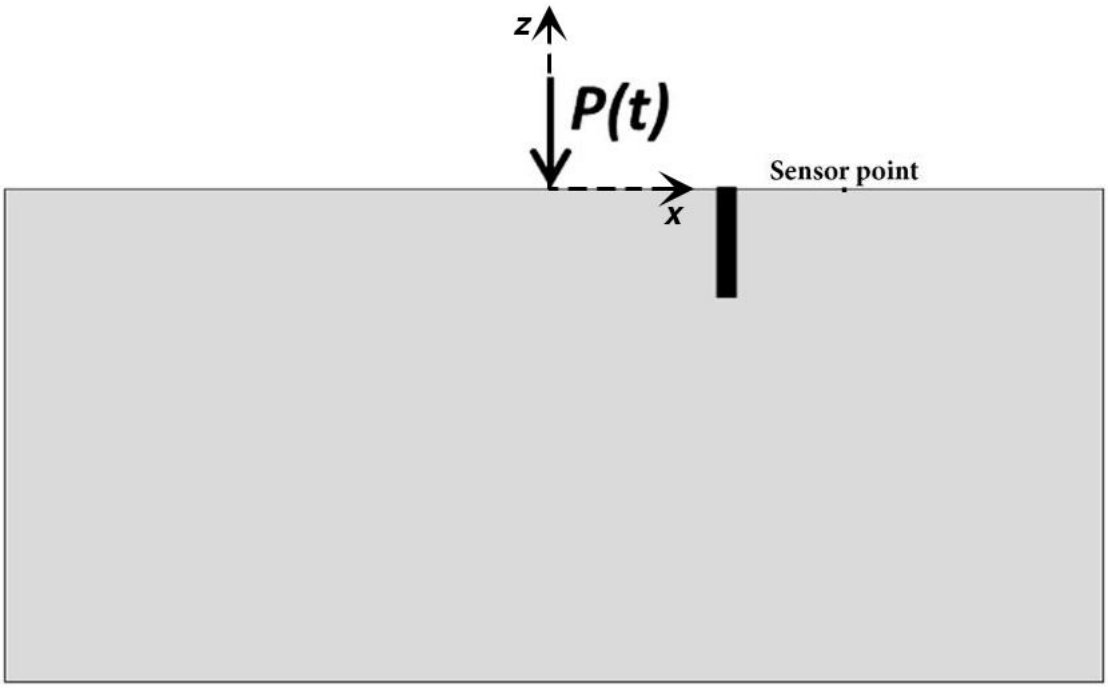

Figure 1. Vertical seismic barrier for protection against vibrations induced by load $P(t)$.

The efficiency of a seismic barrier (i.e., its capability of decreasing the amplitudes of displacements and accelerations) is determined by the properties of materials forming the barrier and the barrier geometry. The effect of material properties has been studied before, e.g., [17]. The present study is one of the first attempts to address the effect of the barrier shape. Previously, only barriers of the simplest (mostly rectangular) cross-sections were considered (e.g., [14–16]). In [18], Brennan et al. present a review of the state of the art in the utilization of soft barriers for protection against seismic hazards. The most sophisticated

cases of seismic protection geometry reported by the authors are a V-shaped protective barrier numerically studied by Flora et al. [3] and a bowl-shaped barrier with an analytical solution reported by Le et al. [19]. Some authors study periodic protective elements as part of the structure basement (e.g., [20]) or that are erected in a vicinity of the structure to be protected (e.g., [15]). In addition to the fact that the available literature about the utilization of barriers for vibration protection is limited to the simplest barrier shapes (i.e., the shape-optimization problem was previously only solved in terms of finding optimal barrier dimensions), there is no practical possibility for a direct quantitative comparison of the observed protective properties to previously published results. The reason for this is that the quantitative data are highly specific to the problem geometry, boundary conditions and loading conditions. At the same time, the protective properties observed below for barriers of simple shape (i.e., a rectangular barrier filled with a single material) are an indication of the protective properties reported in the available literature. It should also be noted that though there are almost no published attempts to optimize the shape of seismic protective barriers, the problem of shape optimization for acoustic protective barriers is much more explored in literature. For example, Duhamel [21] utilizes a genetic algorithm for the shape optimization of noise barriers.

2. Numerical Model

Consider the 2D generalized plane-strain problem (Figure 1) for a halfplane with a barrier of an arbitrary shape. The motion within the halfplane is given by the Lame equation for displacements u_i in the directions x_i:

$$\rho u_{i,tt} = (\lambda + \mu) u_{j,ji} + \mu u_{i,jj}, \tag{1}$$

where μ and ν are the material Lame parameters and ρ is the material mass density. Stresses are coupled with strains by Hooke's law:

$$\sigma_{ij} = \lambda \delta_{ij} u_{k,k} + \mu \left(u_{i,j+} u_{j,i} \right), \tag{2}$$

At $t = 0$, the halfplane is stress-free, and the velocity field is zero everywhere in the plane:

$$\sigma_{ij}\big|_{t=0} = u_{,t}|_{t=0} = 0. \tag{3}$$

The load $P(t)$ is applied as a concentrated force at the surface at $x = 0$. The time dependence of the force is given graphically in Figure 2. The force amplitude P_{peak} = 1000 N.

$$\sigma_{xz}|_{z=0} = 0; \ \sigma_{zz}|_{z=0} = P(t)\delta(x). \tag{4}$$

This problem (1–4) is solved numerically by utilizing the finite-element method (FEM) [17]. To study the interaction of the incident waves with a barrier, a transient dynamic solution accounting for inertia effects should be employed. Herein, the LS-DYNA commercial FEM software [22] was used to solve the dynamic linear-elastic problem of surface wave propagation within the studied domain, taking advantage of explicit time integration.

Solutions for various shapes of a protective barrier are compared with the reference solution, which corresponds to the case when no protective barrier between the source and the sensor point is installed. The reference configuration represents the well-studied 2D Lamb's outer problem [23,24]. The existence of the exact analytical solution for Lamb's outer problem provides the possibility of verifying the accuracy of the numerical FEM approach.

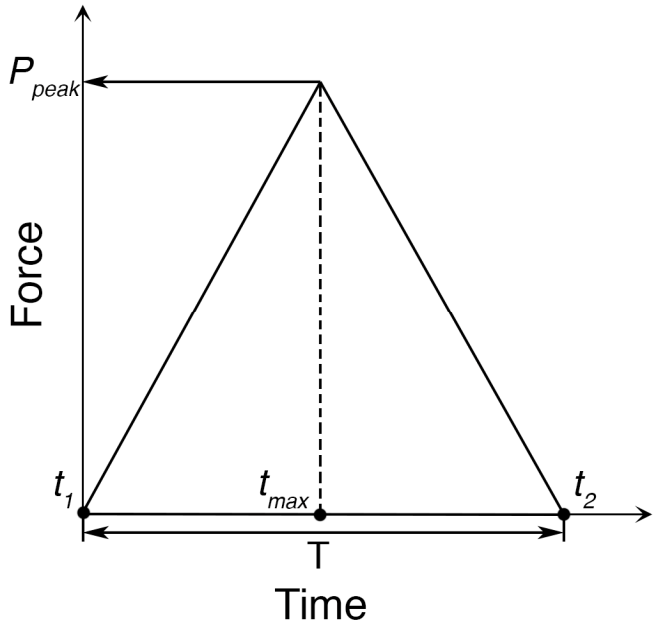

Figure 2. Temporal shape of $P(t)$ used in simulations.

The analytical solution for Lamb's problem with the $P(t)$ given in Figure 2 can be found as a convolution of the Lamb's solution [23–25] for the Dirac delta function with $P(t)$ [26,27]. For a point force applied at the surface and given by:

$$F_x(x,t) = P_h\delta(x)\delta(t);\ F_z(x,t) = P_v\delta(x)\delta(t), \tag{5}$$

where F_x and F_y are the horizontal and vertical components of the force (see Figure 1), P_h and P_v are the corresponding force amplitudes in the horizontal and vertical directions and $\delta()$ being the Dirac delta function, the solution for displacements at the plane surface can be obtained; for example, following Kausel [24]. In (6)–(9), the solution is given separately for the vertical (u_{zz}, u_{zx}) and horizontal (u_{xx}, u_{xz}) components of total displacement caused by the horizontal and the vertical component of the surface load:

$$u_{xx} = \frac{P_h\beta}{\pi\mu|x|}\begin{cases} 0,\ for\ \tau < a \\ \frac{4\tau^2\left(1-\tau^2\right)\sqrt{\tau^2-a^2}}{\left(2\tau^2-1\right)^4+16\tau^4(\tau^2-a^2)(1-\tau^2)},\ for\ a \le \tau \le 1 \\ \frac{-\sqrt{\tau^2-1}}{\left(2\tau^2-1\right)^2+4\tau^2\sqrt{\tau^2-a^2}\sqrt{\tau^2-1}},\ for\ \tau > 1 \end{cases} \tag{6}$$

for displacements in the horizontal (or x) direction caused by the horizontal component of the surface-loading force. Displacements in the vertical (or z) direction caused by the force applied in the vertical direction are:

$$u_{zz} = \frac{P_v\beta}{\pi\mu|x|}\begin{cases} 0,\ for\ \tau < a \\ \frac{-\left(2\tau^2-1\right)^2\sqrt{\tau^2-a^2}}{\left(2\tau^2-1\right)^4+16\tau^4(\tau^2-a^2)(1-\tau^2)},\ for\ a \le \tau \le 1 \\ \frac{-\sqrt{\tau^2-a^2}}{\left(2\tau^2-1\right)^2+4\tau^2\sqrt{\tau^2-a^2}\sqrt{\tau^2-1}},\ for\ \tau > 1 \end{cases} \tag{7}$$

Displacements in the horizontal direction induced by the vertical component of the force are:

$$u_{xz} = \frac{P_v\beta}{\pi\mu|x|}\begin{cases} \frac{2\tau\left(2\tau^2-1\right)\sqrt{\tau^2-a^2}\sqrt{1-\tau^2}}{\left(2\tau^2-1\right)^4+16\tau^4(\tau^2-a^2)(1-\tau^2)},\ for\ a \le \tau \le 1 \\ \frac{\pi\left(2\tau_R^2-1\right)^3}{4\left(1-4\tau_R^2+8\tau_R^6(1-a^2)\right)}\ \delta(\tau-\tau_R),\ else \end{cases} \tag{8}$$

Displacements in the vertical direction induced by the horizontal component of the force are:

$$u_{zx} = -\frac{P_h \beta}{\pi \mu |x|} \begin{cases} \frac{2\tau\left(2\tau^2-1\right)\sqrt{\tau^2-a^2}\sqrt{1-\tau^2}}{\left(2\tau^2-1\right)^4+16\tau^4(\tau^2-a^2)(1-\tau^2)}, \ for\ a \le \tau \le 1 \\ \frac{\pi\left(2\tau_R^2-1\right)^3}{4\left(1-4\tau_R^2+8\tau_R^6(1-a^2)\right)}\,\delta(\tau-\tau_R), \ else \end{cases} \quad (9)$$

In the equations above, $\tau = \frac{t\beta}{|x|}$, $\tau_R = \frac{\beta}{C_R}$, $a = \frac{\beta}{\alpha} = \frac{1-2\nu}{2(1-\nu)}$, where α and β are the longitudinal and transversal wave speeds and C_R is the Rayleigh wave speed. The resulting displacement for any point on the halfspace surface at any time can be obtained as the sum of the above displacements (i.e., $u = u_{zz} + u_{zx} + u_{xx} + u_{xz}$).

Obviously, making use of the above explicit solution for displacements and by performing convolutions for time and the x-coordinate along the surface, one can obtain surface displacements for an arbitrary system of forces, each having an arbitrary time profile, applied on the surface of the studied halfspace. Performing the convolution with the time profile of the point load (given in Figure 2), an exact analytical solution for the reference configuration of the problem (no barrier) will be obtained. Figure 3 plots the comparison between the exact analytical solution and the corresponding numerical solution of the same problem. The observed remarkable coincidence between the exact and the numerical result confirms the applicability of the developed numerical approach to accurately solve the problem of the propagation of elastic waves within the halfplane. The same numerical model was utilized to calculate the amplitudes of displacements and accelerations at a sensor point in the case of a halfspace with a barrier.

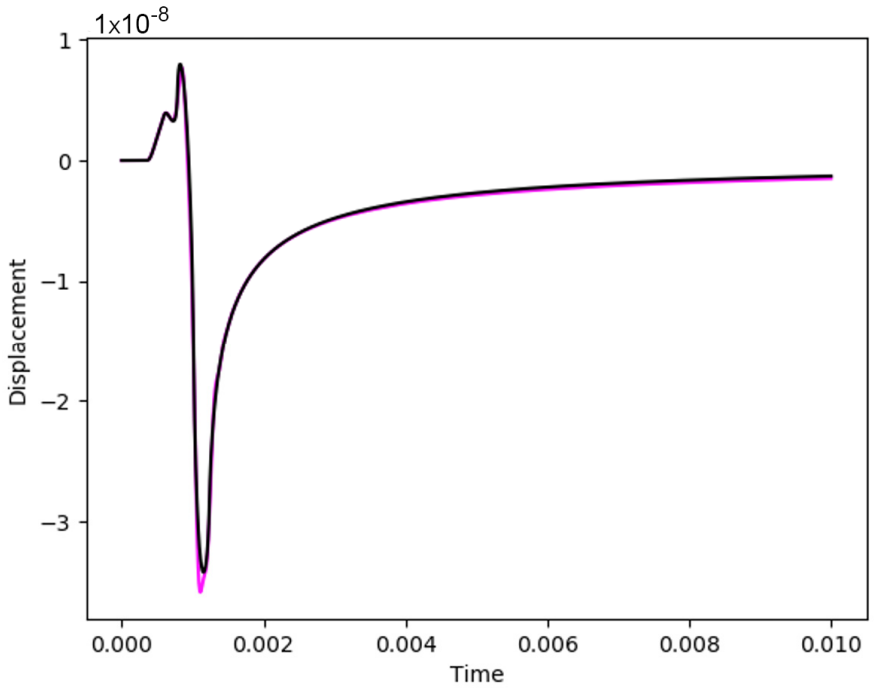

Figure 3. Comparison of displacement history at the sensor point for the exact analytical solution (black line) and the results of FEM numerical simulations (red line) for the reference configuration (no barrier).

Unfortunately, there is no possibility of developing an exact analytical solution for the more complicated problem of the interaction between a wave and an inclusion within a halfplane. The developed numerical model was validated in comparison to the exact analytical solution in the case of no seismic barrier (or, equally, a seismic barrier with properties similar to the ones in the surrounding media). It is demonstrated that the numerical approach can accurately simulate the propagation of dynamic waves, including

bulk waves and surface waves (i.e., Rayleigh waves). It is expected that the same model, for which the properties of the material are altered for some locations, should still accurately simulate the propagation of elastic waves in a media with a seismic barrier.

The load duration T is chosen to be equal to the time needed for the fastest (longitudinal) wave to travel a distance equal to the barrier depth in the material representing the halfspace. There is no doubt that the load duration will significantly affect the wave interaction with a barrier of a prescribed geometry and, hence, will have a substantial impact on the effective barrier protective properties. It is apparent that barriers with sizes significantly smaller than the oncoming wave wavelength cannot have any notable influence on the passing wave. Waves with wavelengths comparable to or smaller than the barrier size can be significantly transformed in the process of interacting with the barrier. Credibly, the waves with wavelengths substantially smaller than the barrier dimensions can be effectively filtered by the barrier with no pronounced dependency on the wavelength. Thereby, the most interesting, from both the theoretical and the practical points of view, is the case of waves with wavelengths comparable to the dimensions of the protective barrier itself.

For each of the tested barrier configurations, the maximum overtime displacement induced by the load $P(t)$ at the sensor point (see Figure 1) is scaled with the magnitude of displacement at the same point for the case with no seismic barrier to obtain the protection factor for the corresponding barrier configuration. Namely:

$$PF = \frac{\max\limits_{t}\left(u\left(x_{sp}, t\right)\right)}{u_{max}^{ref}}, \tag{10}$$

where x_{sp} gives the location of the sensor point, $u(x,t)$ gives the time history of the total displacement at a point with location x and u_{max}^{ref} gives the magnitude of displacement at the sensor point for a reference configuration with no barrier.

For example, a protection factor equal to 2.0 means that the magnitude of displacements in the sensor point is reduced by a factor of 2. The aim of this study is to identify barrier shapes that provide the maximum possible protection, i.e., find the barrier's geometric shape that maximizes the protection factor. Within the framework of the 2D plane-strain problem, it is assumed that the barrier can occupy an area of 1.0 m $\times$ 2.0 m. Finite-element mesh consists of quadratic elements, with the element side equal to 1/3 dm, which gives a domain of 30 $\times$ 60 elements for the seismic barrier area. The domain is divided into clusters of 2 $\times$ 2 elements each, and the barrier area is represented by a 15 $\times$ 30 array of clusters. Each of the 450 clusters can be occupied by either a material with the same properties as the halfplane or by another material (barrier material)—see Figure 4. This means that a barrier can be represented as a binary vector in 450-dimensional space. The medium is simulated as a linear elastic material with the properties typical of soil: elastic modulus, E = 30 MPa; density, ρ = 1750 kg/m^3; Poisson's ratio, ν = 0.3. The material representing the barrier has properties typical of concrete: E = 30 GPa; ρ = 2400 kg/m^3; Poisson's ratio, ν = 0.35.

Initially, an attempt to "guess" a good (providing maximized protection factor) barrier shape was performed. The hypothesis was that adding "scatters" to a simple rectangular-shaped seismic barrier can significantly improve its efficiency. Also, several periodic configurations were tested. Table 1 shows some of the tested barrier shapes with their corresponding protection factors.

Case 1 in Table 1 corresponds to a simple rectangular shape of a seismic barrier (securing a protection factor of 2.2). Case 11 corresponds to the domain completely filled with concrete, with a protection factor of 2.64, being the maximum PF observed at that stage. It is concluded that, within the framework of the problem solved, there is most probably impossible to design a seismic barrier with a PF exceeding the one for the entire domain filled with concrete.

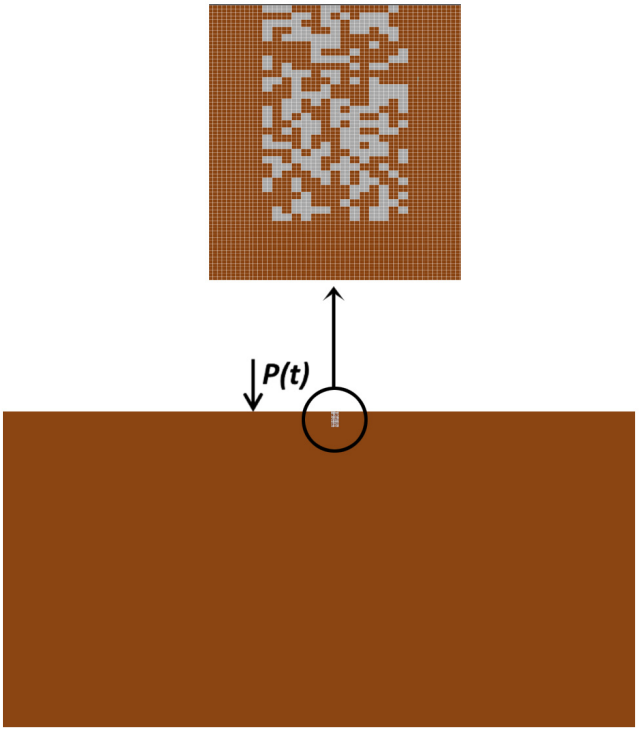

Figure 4. Finite-element discretization and randomly generated barrier geometry.

Table 1. Several of the tested seismic barrier shapes and the computed corresponding protection factors (PFs). Larger protection factors correspond to better protective properties. The brown material corresponds to soil (with the same properties as the surrounding medium) and the gray material corresponds to concrete.

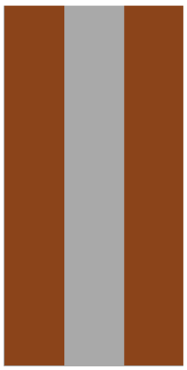		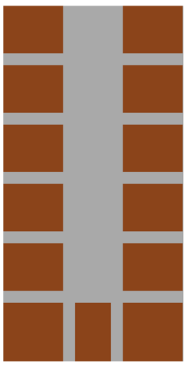	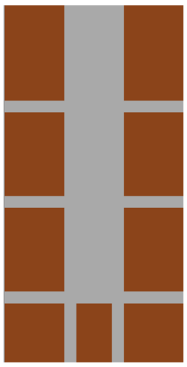	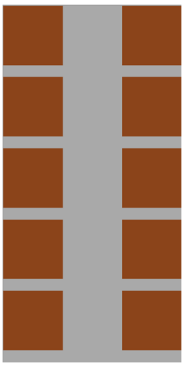	
1. PF = 2.19	2. PF = 2.0	3. PF = 1.82	4. PF = 2.03	5. PF = 2.14	6. PF = 2.23
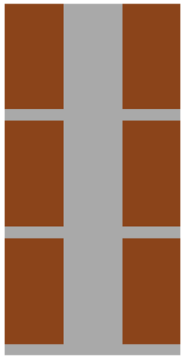	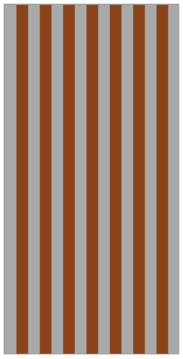	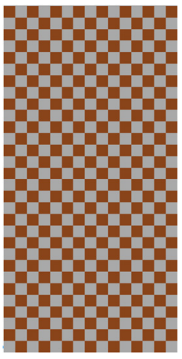	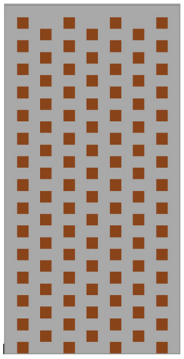	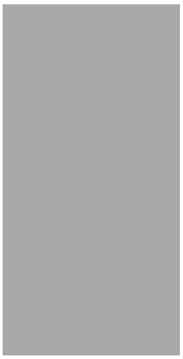	
7. PF = 2.24	8. PF = 1.46	9. PF = 1.98	10. PF = 2.22	11. PF = 2.64	

3. Genetic Algorithm

To reaffirm the conclusion of the previous section and to develop a method for finding an optimal geometric configuration for similar problems (for example, for the case of several different materials that could be used to form a barrier), some method to evaluate the optimal or close-to-optimal configuration of a seismic barrier is needed. This paper is not studying the case of more than one material utilized to form the barrier (in addition to the material of the surrounding media), but this can be explored in the following work. Calculation of the PF for a given geometric configuration of a barrier requires around 5 min of processor time on a high-performance computer system. Obviously, there is no practical possibility of calculating the PF for every possible configuration of a barrier (2^{450} possible configurations). To find "good" geometric shapes for a seismic barrier, it was decided to employ a genetic algorithm (see, e.g., [21,28]) to initiate a process for the evolutionary development of barrier geometric configurations that converges to a configuration with the maximum PF possible. The idea of a genetic algorithm is to mimic the principles of natural selection and genetic inheritance to optimize barrier configurations with respect to protective properties over successive generations. Figure 5 gives the basic scheme of a genetic algorithm.

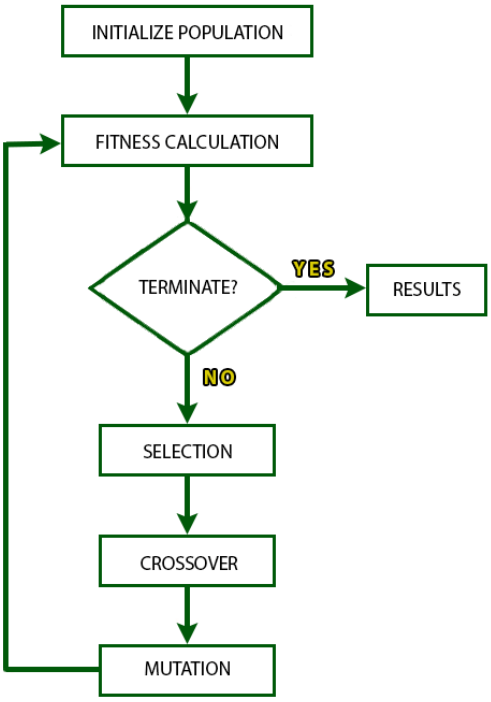

Figure 5. The basic scheme of a genetic algorithm.

Initially, a population of diverse geometric configurations is randomly generated. Alternatively, if there are assumptions about how a "good" seismic barrier configuration should look, these can be used for the generation of the initial population. Every species (barrier configuration) in the population is evaluated using the previously described numerical method to evaluate the PF. For the problem being solved, the PF serves as a fitness function that quantifies the performance of a given barrier shape.

Once the protection factors are calculated, through the process of selection, configurations with higher PFs are chosen as parents for the next generation. The selected barrier configurations undergo genetic operations, including crossovers and mutations, mimicking genetic recombination and variation. Crossover involves combining the geometries of two parent configurations to create a species for the new generation.

Mutation introduces small random changes into the geometry to explore new possibilities. This is implemented by switching materials in a random position inside a barrier.

Combining the operations of crossover and mutation, a new population with the same number of species is generated. The species (barrier geometry) with the highest PF in the previous generation is taken to the next generation unchanged to guarantee that the maximum PF is a non-decreasing function of evolution time.

The process of selection, crossover, and mutation is repeated iteratively. As the generations progress, the population tends to converge toward more optimal configurations, driven by the improvement in the PF. By iteratively applying these genetic operators and evaluating the PF of the resulting configurations, the genetic algorithm explores and refines the space of possible geometric configurations, ultimately converging toward those that exhibit maximum possible protective properties.

4. Implementation of the Genetic Algorithm

Initial population. There are no constraints imposed on the possible shape of the barrier. This means that there are no "prohibited" configurations for the barrier, and any shape can be potentially achieved in the process of evolution. To receive the results presented below, the population (i.e., barrier shapes) for the first generation is generated randomly. This means that every point within a barrier (see Figure 4) is assigned a material with either the properties of concrete or soil with equal probability. This results in approximately equal fractions of soil and concrete within the initial barrier configurations. There is also the possibility of using different fractions of concrete and soil within the initial population. To investigate the convergence of the developed algorithm by demonstrating the independence of the evolution results on the variation of the initial population, computations were performed for various initial fractions of concrete (see Table 2). It was found that the final result of the GA evolution for this problem is not significantly affected by the initial fraction of concrete. For equal fractions of concrete and soil, the GA convergence is slightly faster. The following results were obtained for an initial population with equal fractions of concrete and soil.

Table 2. Examples of initial configurations of barriers with various fractions of concrete. The brown material corresponds to soil (with the same properties as the surrounding medium) and the gray material corresponds to concrete.

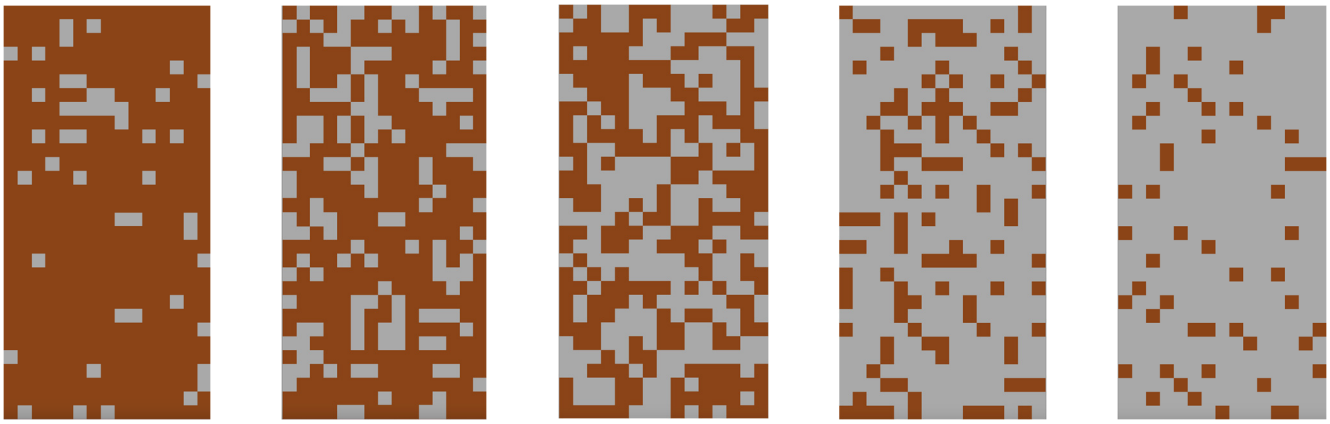

10% of concrete	30% of concrete	50% of concrete	70% of concrete	90% of concrete

Population size. Calculations were performed for different numbers (4, 8, 12, 24, 40) of species (barrier geometries) in a population. It was found empirically that the final result of the GA evolution for this problem is not significantly affected by the population size. It was found empirically that for the problem solved and the computational system utilized for these simulations, having 8–12 species in a population provides the fastest possible convergence. The below results were obtained for a population of 12 species.

Calculation of fitness. For each individual species, fitness is calculated utilizing (10) and with the results of the described above FEM solution (Figure 4), solving the problem

of (1)–(4). Fitness is determined by the protection factor, which reflects the ability of the definite barrier geometry to decrease the amplitudes of vibrations at the surface behind the barrier.

Selection. Following the calculation of fitness for each species in the generation, half of the species with the lowest fitness is dismissed. The other half of the species is used to produce the next generation via crossover and mutation. The species with the highest fitness in the generation is taken to the next generation unchanged to guarantee that the fitness is never decreasing through the evolutionary process.

Crossover. A very simple approach to performing a crossover between two species was adopted: the child's geometry takes the upper half of the geometry from one parent and the lower half of geometry from the other parent. Random crossover between the higher-fitness species of the previous generation was used to create the species of the new generation (except for the species with the highest fitness from the previous generation, which is always copied to the next generation).

Mutation. Mutation involves switching the material (soil→concrete or concrete→soil) at a random location of a barrier. It was found empirically that switching materials at more than one point at a time does not have any benefit and impedes the convergence. The probability of mutation is ½.

Genetic algorithm. Once the new generation is produced following selection, crossover and mutation, the fitness is calculated for this new generation, and then the process is looped until the condition for termination is fulfilled. For the computations presented below, the process was terminated once the predefined number of generations was reached (typically 1000 generations). As seen from the results presented below, the fitness is still improving at the typical termination time, but the observed changes to the barrier geometry are minor and there is no major benefit to performing computations for additional generations. Alternatively, the termination condition can be the achievement of a definite fitness value or a significant decrease in the convergence rate.

5. Results

Figure 6 plots the observed evolution of fitness (maximum protection factor) for the genetic algorithm evolution that was started from a randomly generated initial population. The same figure shows that the final (biggest PF) configuration of seismic barrier geometry gives a protection factor of 2.84. This is significantly higher than the protection factor for a barrier with the entire domain filled with concrete (PF = 2.64, see Table 1), which was previously believed to provide the biggest PF possible.

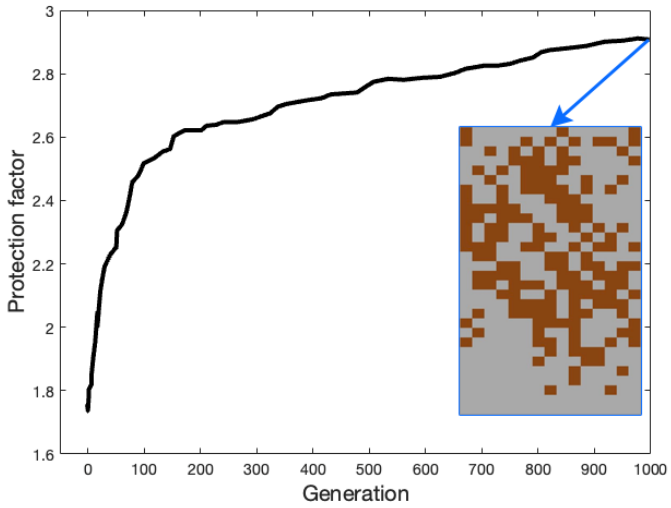

Figure 6. Evolution of fitness (PF) during the genetic algorithm evolution. The picture shows the final barrier shape securing a protection factor of 2.84.

In order to study the convergence and repeatability, the developed GA evolution was executed several times, starting from a randomly generated initial population. A total of more than 50 GA runs were executed, all resulting in very similar optimal barrier geometries after 1000 generations. Some of the final shapes obtained and their corresponding protection factors are presented in Table 3.

Table 3. Final shapes and their corresponding protection factors for three GA evolutions with a randomly generated initial population. Comparison with the protection factor for a barrier with the entire domain filled with concrete.

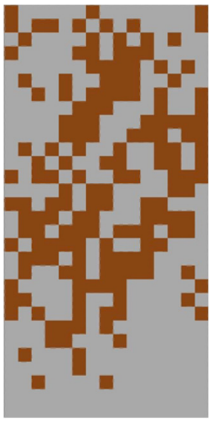		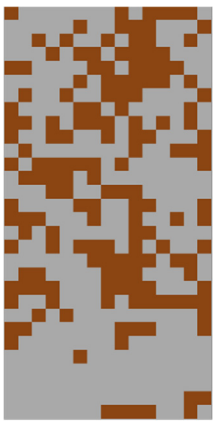	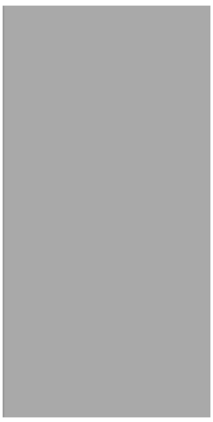
GA run 1. PF = 2.84	GA run 2. PF = 2.75	GA run 3. PF = 2.82	100% concrete. PF = 2.64

An attempt was made to initiate a new GA evolution using final barrier shapes from previous evolutions as an initial population. This attempt is also important for evaluating the optimal shape as, typically, there is still an increase in the fitness at the termination time of a GA starting from a random initial population (Figure 6). Figure 7 shows the resulting evolution of the PF and the final barrier shape obtained, with the PF = 2.92.

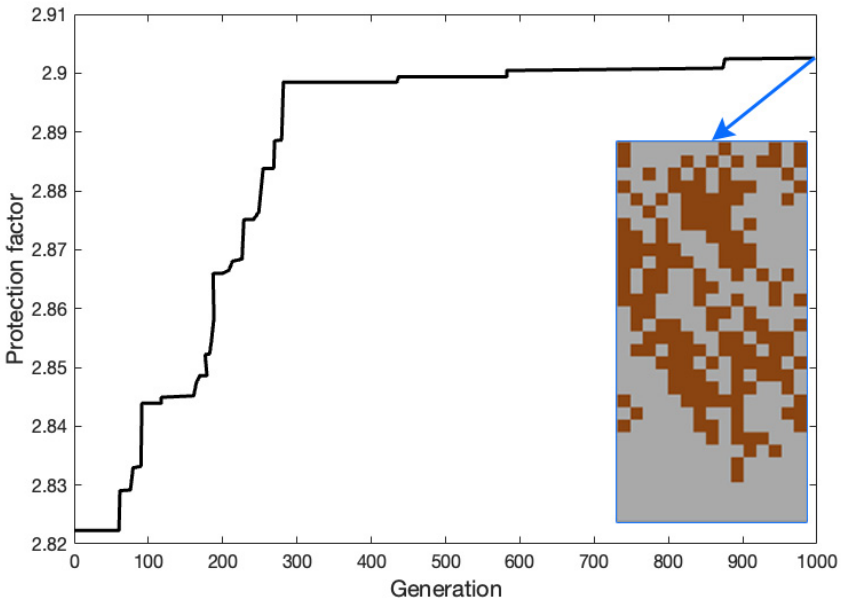

Figure 7. Evolution of fitness (PF) during the genetic algorithm evolution using barrier shapes from Table 2 as the initial population. The picture shows the final barrier shape securing a protection factor of 2.92.

6. Conclusions and Discussion

Utilization of a GA provided the possibility of revealing barrier shapes with protection factors significantly exceeding the protection factor for a homogeneous barrier entirely filled with concrete, which was previously believed to give the highest possible PF. All of the obtained "good" barrier shapes are very similar, which is an indication of the GA convergence and repeatability. The barrier shapes with high PFs have concrete concentrated at the lower end of the barrier from the direction of the wave arrival (left). The rest of the barrier resembles a layered structure inclined at 45°. It is not yet clear what diffraction processes lead to this kind of structure. To understand these processes, presumably a finer discretization of the barrier domain is required. The observed asymmetry of the optimized barrier is the result of the essential asymmetry of the studied problem. For most practical cases of seismic protection, the direction from which the seismic wave is expected to arrive is known. However, if this direction is not known, the constraint on the barrier symmetry should be imposed before the shape optimization is initiated. This present work does not explore this case.

Unfortunately, increasing the barrier discretization density implies a significant increase in both the time needed to obtain the numerical solution for a given barrier shape and the number of PF calculations for convergence of the GA. For example, the calculations presented in Figure 6 (single run of a GA evolution for 1000 generations) required a week of computational time on a high-performance computer system. For this reason, any significant complication of the existing problem will result in the practical impossibility of obtaining the GA convergence.

At the same time, it is believed that there exists a possibility to significantly reduce the number of PF computations needed for the evaluation of "good" barrier geometric shapes. This will require a substantial modification of the GA or its substitution by another generative algorithm (e.g., indirect evolutionary algorithm [29]).

A crucial aspect of the interaction between mechanical waves and inclusions is the inherent multiscale character of this phenomenon. The dimensions of the geometric features within these inclusions are closely tied to the frequency of the incident waves with which the inclusions can effectively interact. Therefore, methods that presuppose the possible existence of certain geometric patterns hold the potential for both significant acceleration of the algorithm convergence and uncovering highly efficient, intricate geometric configurations. The compositional pattern-producing network (CPPN) (see, e.g., [30]) is one of the generative approaches that can be used to efficiently construct the optimal geometric shapes for inclusions interacting with waves. At this stage, it is not possible to directly compare the performance of the developed genetic algorithm to other available generative algorithms as this will require the implementation of these algorithms to solve the same problem and the following long-term simulations.

It should also be noted that a wide variety of fundamental and engineering problems require the optimization of shape in the case when it is not possible to parametrize this shape with several parameters. For example, this kind of problem appears in the construction of various protective structures, in the design of metamaterials, in materials engineering, etc. In most cases, the evaluation of optimal geometric shape results in an attempt to predict what the optimal shape should be. As demonstrated in this research, even a very simple GA can be efficiently applied to evaluate extremely nontrivial geometric shapes that cannot be parameterized.

Author Contributions: Conceptualization, V.B.; Methodology, V.B.; Software, A.M.; Validation, A.M.; Formal analysis, S.V.K.; Investigation, V.B. and A.M.; Writing—original draft, V.B.; Writing—review & editing, V.B.; Supervision, S.V.K. All authors have read and agreed to the published version of the manuscript.

Funding: This research was partly funded by the Ministry of Science and Higher Education of the Russian Federation as part of the World-class Research Center program: Advanced Digital Technologies (contract No. 075-15-2022-311 dated 20 April 2022).

Data Availability Statement: The data presented in this study are available on request from the corresponding author.

Conflicts of Interest: The authors declare no conflict of interest.

References

1. Adam, M.; Estorff, O. Reduction of train-induced building vibrations by using open and filled trenches. *Comput. Struct.* **2005**, *83*, 11–24. [CrossRef]
2. Li, T.; Su, Q.; Kaewunruen, S. Seismic metamaterial barriers for ground vibration mitigation in railways considering the train-track-soil dynamic interactions. *Constr. Build. Mater.* **2020**, *260*, 119936. [CrossRef]
3. Flora, A.; Lombardi, D.; Nappa, V.; Bilotta, E. Numerical analyses of the effectiveness of soft barriers into the soil for the mitigation of seismic risk. *J. Earthq. Eng.* **2018**, *22*, 63–93. [CrossRef]
4. Mu, D.; Shu, H.; Zhao, L.; An, S. A Review of Research on Seismic Metamaterials. *Adv. Eng. Mater.* **2020**, *22*, 1901148. [CrossRef]
5. Brûlé, S.; Enoch, S.; Guenneau, S. Emergence of seismic metamaterials: Current state and future perspectives. *Phys. Lett. A* **2020**, *384*, 126034. [CrossRef]
6. Geng, Q.; Zhu, S.; Chong, K.P. Issues in design of one-dimensional metamaterials for seismic protection. *Soil Dyn. Earthq. Eng.* **2018**, *107*, 264–278. [CrossRef]
7. Kacin, S.; Ozturk, M.; Sevim, U.K.; Mert, B.A.; Ozer, Z.; Akgol, O.; Unal, E.; Karaaslan, M. Seismic metamaterials for low-frequency mechanical wave attenuation. *Nat. Hazards* **2021**, *107*, 213–229. [CrossRef]
8. Albino, C.; Godinho, L.; Amado-Mendes, P.; Alves-Costa, P.; Dias-da-Costa, D.; Soares, D. 3D FEM analysis of the effect of buried phononic crystal barriers on vibration mitigation. *Eng. Struct.* **2019**, *196*, 109340. [CrossRef]
9. Sun, F.; Xiao, L.; Bursi, O.S. Optimal design and novel configuration of a locally resonant periodic foundation (LRPF) for seismic protection of fuel storage tanks. *Eng. Struct.* **2019**, *189*, 147–156. [CrossRef]
10. Wenzel, M.; Bursi, O.S.; Antoniadis, I. Optimal finite locally resonant metafoundations enhanced with nonlinear negative stiffness elements for seismic protection of large storage tanks. *J. Sound Vib.* **2020**, *483*, 115488. [CrossRef]
11. Rezaie, A.; Rafiee-Dehkharghani, R.; Dolatshahi, K.M.; Mirghaderi, S.R. Soil-buried wave barriers for vibration control of structures subjected to vertically incident shear waves. *Soil Dyn. Earthq. Eng.* **2018**, *109*, 312–323. [CrossRef]
12. Jesmani, M.; Fallahil, M.A.; Kashani, H.F. Effects of geometrical properties of rectangular trenches intended for passive isolation in sandy soils. *Earth Sci. Res.* **2012**, *1*, 137–151. [CrossRef]
13. Kim, S.H.; Das, M.P. Artificial seismic shadow zone by acoustic metamaterials. *Mod. Phys. Lett. B* **2013**, *27*, 1350140. [CrossRef]
14. Palermo, A.; Krödel, S.; Marzani, A.; Daraio, C. Engineered metabarrier as shield from seismic surface waves. *Sci. Rep.* **2016**, *6*, 39356. [CrossRef] [PubMed]
15. Gupta, A.; Sharma, R.; Thakur, A.; Gulia, P. Metamaterial foundation for seismic wave attenuation for low and wide frequency band. *Sci. Rep.* **2023**, *13*, 2293. [CrossRef] [PubMed]
16. Bratov, V.A.; Ilyashenko, A.V.; Kuznetsov, S.V.; Lin, T.K.; Morozov, N.F. Homogeneous horizontal and vertical seismic barriers: Mathematical foundations and dimensional analysis. *Mater. Phys. Mech.* **2020**, *44*, 61–65.
17. Bratov, V.; Kuznetsov, S.; Morozov, N. Seismic barriers filled with solid elastic and granular materials. *Comp. Anal. Math. Mech. Solids* **2022**, *27*, 1761–1770. [CrossRef]
18. Brennan, A.J.; Klar, A.; Madabhushi, S. Mitigation of Seismic Accelerations by Soft Materials Embedded in the Ground. *Proc. Inst. Civ. Eng.-Ground Improv.* **2019**, *3*, 117–140.
19. Le, T.; Lee, V.W.; Luo, H. Out of plane (SH) soil-structure interaction: A shear wall with rigid and flexible ring foundation. *Earth Sci.* **2016**, *29*, 44–55. [CrossRef]
20. Martakis, P.; Aguzzi, G.; Dertimanis, V.K.; Chatzi, E.N.; Colombi, A. Nonlinear periodic foundations for seismic protection: Practical design, realistic evaluation and stability considerations. *Soil Dyn. Earthq. Eng.* **2021**, *150*, 106934. [CrossRef]
21. Duhamel, D. Shape optimization of noise barriers using genetic algorithms. *J. Sound Vib.* **2006**, *297*, 432–443. [CrossRef]
22. ANSYS Company. *LS-DYNA Manual R12.0*; Livermore Software Technology (LST); ANSYS Company: Canonsburg, PA, USA, 2020.
23. Lamb, H. On the propagation of tremors over the surface of an elastic solid. *Philos. Trans. R. Soc. Lond. A* **1904**, *203*, 1–42.
24. Kausel, E. Lamb's problem at its simplest. *Proc. R. Soc. A Math. Phys. Eng. Sci.* **2012**, *469*, 20120462. [CrossRef]
25. Eringen, A.C.; Suhubi, E.S. *Elastodynamics, Volume II: Linear Theory*; Academic Press: New York, NY, USA, 1975.
26. Bratov, V.A.; Kuznetsov, S.V.; Morozov, N.F. Lamb's problems and related problems of dynamics. *J. Appl. Math. Mech.* **2022**, *86*, 451–469.
27. Morozov, N.F.; Bratov, V.A.; Kuznetsov, S.V. Seismic barriers for protection against surface and head waves: Multiple scatters and metamaterials. *Mech. Solids* **2021**, *56*, 911–921. [CrossRef]
28. Mirjalili, S. Genetic Algorithm. In *Evolutionary Algorithms and Neural Networks. Studies in Computational Intelligence*; Springer: Cham, Switzerland, 2019; Volume 780.

29. Hart, E.; Le Goff, L.K. Artificial evolution of robot bodies and control: On the interaction between evolution, learning and culture. *Philos. Trans. R. Soc. B* **2022**, *377*, 20210117. [CrossRef] [PubMed]
30. Stanley, K.O.; D'Ambrosio, D.B.; Gauci, J. A hypercube-based encoding for evolving large-scale neural networks. *Artif. Life* **2009**, *15*, 185–212. [CrossRef]